MARVEL domain containing CMTM4 affects CXCR4 trafficking

Alexandra Bona[a,b,*], Michael Seifert[a], Roland Thünauer[c,d], Kyra Zodel[e], Ian J. Frew[e,f,g], Winfried Römer[g,h,i], Gerd Walz[a,g], and Toma A. Yakulov[a,*]

[a]Renal Division and [e]Department of Medicine I, Medical Center, Faculty of Medicine, University of Freiburg, 79106 Freiburg, Germany; [b]Spemann Graduate School of Biology and Medicine (SGBM), University of Freiburg, 79104 Freiburg, Germany; [c]Technology Platform Light Microscopy and Image Analysis (TP MIA), Leibniz Institute for Experimental Virology (HPI), 20251 Hamburg, Germany; [d]Advanced Light and Fluorescence Microscopy (ALFM) Facility, Centre for Structural Systems Biology (CSSB), 22607 Hamburg, Germany; [f]German Cancer Consortium (DKTK), Partner Site Freiburg, and German Cancer Research Center (DKFZ), 69120 Heidelberg, Germany; [g]Signalling Research Centres BIOSS and CIBSS, [h]Freiburg Institute for Advanced Studies (FRIAS), and [i]Faculty of Biology, Albert-Ludwigs-University Freiburg, 79104 Freiburg, Germany

ABSTRACT **The MARVEL proteins CMTM4 and CMTM6 control PD-L1, thereby influencing tumor immunity. We found that defective zebrafish *cmtm4* slowed the development of the posterior lateral line (pLL) by altering the Cxcr4b gradient across the pLL primordium (pLLP). Analysis in mammalian cells uncovered that CMTM4 interacted with CXCR4, altering its glycosylation pattern, but did not affect internalization or degradation of CXCR4 in the absence of its ligand CXCL12. Synchronized release of CXCR4 from the endoplasmic reticulum revealed that CMTM4 slowed CXCR4 trafficking from the endoplasmic reticulum to the plasma membrane without affecting overall cell surface expression. Altered CXCR4 trafficking reduced ligand-induced CXCR4 degradation and affected AKT but not ERK1/2 activation. CMTM4 expression, in contrast to that of CXCR4, correlated with the survival of patients with renal cell cancer in the TCGA cohort. Furthermore, we observed that *cmtm4* depletion promotes the separation of cells from the pLLP cell cluster in zebrafish embryos. Collectively, our findings indicate that CMTM4 exerts general roles in the biosynthetic pathway of cell surface molecules and seems to affect CXCR4-dependent cell migration.**

Monitoring Editor
Rachel Brewster
University of Maryland, Baltimore County

Received: May 4, 2022
Revised: Aug 15, 2022
Accepted: Aug 24, 2022

This article was published online ahead of print in MBoC in Press (http://www.molbiolcell.org/cgi/doi/10.1091/mbc.E22-05-0152) on August 31, 2022.

Conflict of interest: The authors declare no competing financial interests.

Author contributions: M.S., A.B., and R.T. performed experiments; K.Z. and I.J.F. analyzed data; R.T., W.R., G.W., T.A.Y., and A.B. designed experiments and interpreted data; A.B., T.A.Y., and G.W. wrote the manuscript.

*Address correspondence to: Alexandra Bona (alexandra.bona@uniklinik-freiburg.de); Toma A. Yakulov (toma.antonov.yakulov@uniklinik-freiburg.de).

Abbreviations used: ACKR3, atypical chemokine receptor 3; CKLF, chemokine-like factor; CMTM, CKLF-like MARVEL transmembrane domain containing; CXCL12, C-X-C motif chemokine ligand 12; CXCR4, C-X-C chemokine receptor type 4; CXCR7, C-X-C chemokine receptor type 7; ERK, extracellular signal-regulated kinase; HEK, human embryonic kidney; HIF1α, hypoxia-inducible factor 1-alpha; MAPK, mitogen-activated protein kinase; MARVEL, myelin and lymphocyte and related proteins for vesicle trafficking and membrane link; PD-L1, programmed death ligand 1; PI3K, phosphatidylinositol 3-kinase; PNGase F, peptide N-glycosidase F; RAB11, Ras-associated binding 11; Rb1, retinoblastoma protein 1; STUB1, STIP1 homology and U-box containing protein 1; TCGA, the cancer genome atlas; Trp53, transformation related protein 53; VHL, von hippel-lindau.

INTRODUCTION

The chemokine-like factor (CKLF)-like MARVEL transmembrane domain containing (CMTM) family members CMTM4 and CMTM6 have been implicated in regulating surface expression of the programmed death-ligand 1 (PD-L1) (Burr *et al*., 2017; Mezzadra *et al*., 2017). CMTM4 and CMTM6 belong to the chemokine-like factor superfamily, consisting of eight CMTM members. Common to all MARVEL domain proteins is an M-shaped topology with four transmembrane-helix regions and cytoplasmic N- and C-terminal regions (Sánchez-Pulido *et al*., 2002). Some of the MARVEL domain proteins have been associated with specialized membrane microdomains and appear to participate in cholesterol-rich membrane apposition effects, such as the biogenesis of vesicular transport carriers or tight junction regulation (Sánchez-Pulido *et al*., 2002).

Depletion of CMTM6 reduced cellular levels of PD-L1 and increased ubiquitylation of PD-L1 by the E3 ligase STUB1. While loss of CMTM6 did not impair PD-L1 export from the endoplasmic reticulum (ER), PD-L1 disappeared from the cell surface in the absence of CMTM6, suggesting that CMTM6 is required for stable expression of PD-L1 at the plasma membrane. Localization studies

identified CMTM6 at the plasma membrane and in RAB11-positive recycling endosomes. In the absence of CMTM6, PD-L1 is targeted for degradation in the lysosome. CMTM4 displays 55% homology to CMTM6 and forms heteromers with CMTM6 (Mezzadra *et al.*, 2017).

Given its importance in regulating PD-L1 expression, we genetically manipulated *cmtm4* expression in zebrafish. We observed that the development of the posterior lateral line primordium (pLLP) and Cxcr4b gradient formation were affected by mutating or depleting zebrafish *cmtm4*. The pLLP represents a cluster of cells that migrate from near the ear to the tail, periodically depositing neuromasts to form the lateral line, a sensory system that helps fish to detect water flow (Dalle Nogare and Chitnis, 2017). The craniocaudal migration of the pLLP is orchestrated by a Cxcr4b gradient with short-lived Cxcr4b at the leading end, competing for Cxcl12a ligand binding and slow turnover of Cxcr4b at the trailing end (Dona *et al.*, 2013); mutation or depletion of either *cxcl12a* or *cxcr4b* interferes with normal lateral line development (Valentin *et al.*, 2007).

The importance of CXCL12/CXCR4 signaling during mammalian embryogenesis is underscored by the perinatal lethality in *Cxcl12* and *Cxcr4* mutant mice that develop severe defects in hematopoiesis, vascularization, and cardiac development (Nagasawa *et al.*, 1996; Zou *et al.*, 1998). CXCR4 is extensively posttranslationally modified, including glycosylation, phosphorylation, ubiquitylation, and sulfation (Busillo and Benovic, 2007). Upon CXCL12 binding, CXCR4 undergoes conformational changes to initiate multiple cellular pathways, including MAPK/ERK and PI3K/AKT signaling (Sadri *et al.*, 2022). Phosphorylation and ubiquitylation initiate internalization and lysosomal degradation of CXCR4 (Marchese, 2014; Caballero *et al.*, 2019).

CXCL12 and CXCR4 are expressed in several cancer types, and increased expression correlates with metastasis and worsened prognosis (Shi *et al.*, 2020). Epigenetic, transcriptional, and posttranscriptional regulation have been implicated in the control of both proteins (Guo *et al.*, 2016). In clear cell renal cell carcinoma, VHL mutations prevent degradation of HIF1α, causing an up-regulation of CXCR4 (Staller *et al.*, 2003).

Analysis in mammalian cells revealed that CMTM4 interacted with CXCR4. Furthermore, CMTM4 altered CXCR4 glycosylation and its response to ligand-induced signaling, likely as a consequence of altered trafficking. Collectively, our findings demonstrate that the function of CMTM4 is not restricted to control PD-L1 expression, but likely controls the trafficking of a broader set of cell surface proteins, including CXCR4.

RESULTS

A zebrafish *cmtm4* mutation retards the development of the pLLP

We first determined the expression pattern of *cmtm4* during zebrafish embryogenesis. In situ hybridization revealed that *cmtm4* expression is restricted to the pronephric tubule, cloaca, posterior and anterior lateral lines, otic vesicle, nares, and hatching gland during the first 3 d of embryogenesis (Supplemental Figure S1). We next generated a CRISPR/Cas9 hypomorphic *cmtm4*$^{\Delta 60/\Delta 60}$ zebrafish mutant lacking 20 N-terminal amino acids and targeted *cmtm4* by morpholino oligonucleotides (MOs) (Supplemental Figure S2, A and B). Both approaches affected migration of the pLLP. To quantify the pLLP migration defect, anatomical landmarks were used to create zones, and proneuromasts deposited in individual zones were counted at 1, 2, and 3 d postfertilization (Figure 1A). Migration of the pLLP was significantly reduced in *cmtm4*$^{\Delta 60/\Delta 60}$ zebrafish embryos and zebrafish embryos treated with a *cmtm4* MO (Figure 1B). Directed craniocaudal migration of the pLLP is orchestrated by a Cxcr4b gradient with short-lived Cxcr4b at the leading end and slow turnover of Cxcr4b at the trailing end (Dona *et al.*, 2013). We analyzed the Cxcr4b lifetime gradient using the *cxcr4b:tFT* zebrafish line (Dona *et al.*, 2013), in which Cxcr4b is fused to a quickly maturing superfolder (sf) GFP and a slowly maturing RFP. The Cxcr4 lifetime gradient was noticeably affected in the CRISPR/Cas9 generated *cmtm4*$^{\Delta 60/\Delta 60}$ zebrafish mutant and after knockdown of *cmtm4*, indicating that *cmtm4* depletion interferes with the formation of a normal Cxcr4b gradient (Figure 1C). The slower Cxcr4b turnover at the trailing end is caused by competition between Cxcr4b and Cxcr7/Ackr3 for the ligand Cxcl12 (Dona *et al.*, 2013). While Cmtm4 could modulate Cxcr4b expression or localization, immunofluorescence in the *cmtm4*$^{\Delta 60/\Delta 60}$ embryos revealed normal expression of Cxcr7/Ackr3, suggesting that Cmtm4 rather modulates Cxcr4b trafficking (Figure 1D).

CXCR4 interacts with CMTM4

We next examined whether CXCR4 interacts with CMTM4. Flag-tagged CMTM4 and CMTM6 were cotransfected with wild-type (WT) CXCR4 into HEK 293T cells; a membrane-bound, myristoylated-palmitoylated version of GFP with a C-terminal Flag (mpGFP.F) served as a negative control. After immune precipitation with anti-Flag, CXCR4 was detected in CMTM4 but not in CMTM6 precipitates (Figure 2A). The interaction with endogenous CXCR4 was confirmed in HeLa cells expressing CMTM4.F after induction with tetracycline (Figure 2B). To test whether the interaction between CXCR4 and CMTM4 occurs at the cell surface, we inserted a V5 tag into the first extracellular loop of CMTM4 (CMTM4.V5L) (Supplemental Figure S2C). HEK 293T cells transfected with CMTM4.V5L together with CXCR4 were incubated with a V5 antibody before cell lysis. After removal of unbound antibody, cells were lysed and subsequently incubated with Dynabeads to immobilize CMTM4.V5L. CMTM4.V5L was detectable in the precipitates, confirming the presence of CMTM4.V5L at the cell surface (Figure 3). Coexpression of the CMTM4.V5L shifted CXCR4 to the lower-molecular-weight form similar to CMTM4.F, indicating that the V5 tag did not affect the overall properties of CMTM4. CXCR4 coimmunoprecipitated with CMTM4.V5L, suggesting an interaction between the two proteins at the cell surface. However, precipitation of CMTM4.V5L predominantly immobilized CXCR4 species with a higher-molecular-weight (≥62 kDa) and a shorter ~37 kDa CXCR4 species. CXCR4 heterogeneity has been described (Lapham *et al.*, 1999, 2002). Although we cannot rule out that the lower CXCR4 species bound to CMTM4 after cell lysis, the interaction with higher-molecular-weight forms of CXCR4 appears to occur at the cell surface. The interaction between CXCR4 and CMTM4 at the cell surface was also supported by affinity purification of CXCR4 from nonpermeabilized cells, using an anti-CXCR4 antibody that recognizes the extracellular N-terminus (Supplemental Figure S3).

CMTM4 modulates CXCR4 protein levels

Coexpression of CMTM4 altered the protein levels of a Flag-tagged version of CXCR4 (CXCR4.F) in transfected HEK 293T cells (Figure 4). While small amounts of CMTM4 tended to increase CXCR4 levels, larger amounts almost completely eliminated the ~45 kDa form of CXCR4, using an anti-Flag antibody to detect CXCR4. A monoclonal antibody directed against CXCR4 revealed that CMTM4 reduced the expression of the ~45 kDa form of CXCR4 and facilitated the accumulation of ~37 kDa species. In contrast, coexpression of CMTM6 had much less of an effect on CXCR4 protein levels, although there was some accumulation of the lower-molecular-weight species of

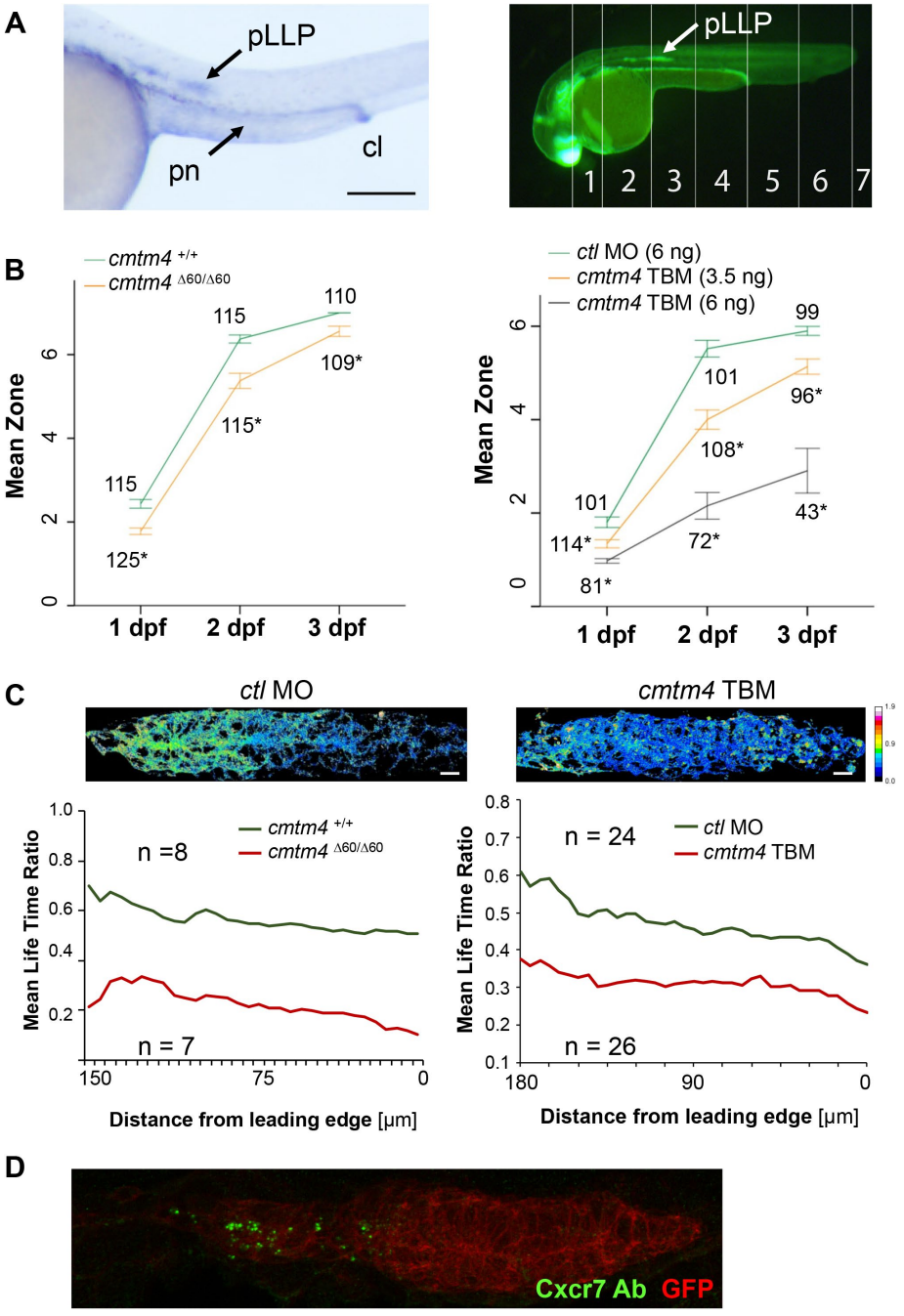

FIGURE 1: Depletion of *cmtm4* in the developing zebrafish embryo affects the development of the pLLP. (A) In situ hybridization for *cmtm4* in zebrafish embryos 36 hours post fertilization (hpf), depicting the position of the pLLP, the pronephros (pn), and the cloaca (cl) (lateral view; scale bar, 200 µm). To analyze the migration of the pLLP and proneuromast deposition, anatomical landmarks were used to create zones in *cldnb:lyn-GFP* transgenic zebrafish. (B) Proneuromasts deposited in individual zones were counted, excluding the terminal proneuromasts. Migration of the pLLP was significantly reduced in *cmtm4*$^{\Delta 60/\Delta 60}$ zebrafish embryos as well as in zebrafish embryos treated with a translation-blocking *cmtm4* MO (*cmtm4* translation-blocking morpholino oligonucleotide [TBM]) in a dose-dependent manner in comparison to control (*ctl*) MO. The inserted numbers depict the numbers of individual zebrafish embryos (mean ± SEM; *, $p < 0.05$). (C) Turnover of Cxcrb4 across the pLLP was determined using the *cxcr4b:tFT* zebrafish line (Dona *et al.*, 2013). The Cxcr4b lifetime gradient was noticeably affected in the *cmtm4*$^{\Delta 60/\Delta 60}$ and TBM-treated zebrafish embryos (*cmtm4* TBM, 5 ng) in comparison to WT or control (*ctl* MO, 5 ng) embryos (Pearson's coefficient for *ctl* MO: $r = 0.267$, $p < 0.001$; Pearson's coefficient for *cmtm4* TBM: $r = 0.173$, $p < 0.001$; scale bars, 10 µm). Statistical analysis was performed using SPSS Statistics 23 (IMDB). The error bars represent the 95% confidence interval. (D) Immunofluorescence for Cxcr7 (green) and GFP (red) in *cmtm4*$^{\Delta 60/\Delta 60}$, *cldnb:lyn-GFP* embryos reveals normal expression and localization of Cxcr7. A representative image from two biological repetitions with at least 30 embryos per staining is shown.

CXCR4 in the presence of CMTM6. These observations suggest that CMTM4, and to a smaller degree CMTM6, affect CXCR4 protein processing.

CMTM4 alters the pattern of CXCR4 glycosylation

The N-terminal extracellular domain of CXCR4 contains two N-linked glycosylation sites (N15, N180 in CXCR4 isoform a, NP_001008540.1); however, their role in ligand binding and human immunodeficiency virus (HIV) entry are controversial (Picard *et al.*, 1997; Zhou and Tai, 1999; Chabot *et al.*, 2000; Huskens *et al.*, 2007). Deglycosylation of CXCR4 by PNGase F suggested that the shift from the ~45 kDa to the ~37 kDa species of CXCR4 in the presence of CMTM4 (Figure 5A) was likely due to the appearance of a partially glycosylated CXCR4 species (Figure 5, B and C).

The ~45 and ~37 kDa CXCR4 species were preserved in the N180A CXCR4 mutant in transfected HEK 293T cells but shifted to less than 37 kDa in the N15A CXCR4 mutant, indicating that N15 is the main glycosylation site in HEK 293T cells (Figure 5D). Noticeably, two lower-molecular-weight CXCR4 species (~37/~32 kDa) were present in the N15A mutant, with the lower band corresponding to the completely deglycosylated species after PNGase F treatment. The upper ~37 kDa band was abolished in the N15A/N180A double CXCR4 mutant, suggesting residual glycosylation of the N15A mutant and the CXCR4 WT in the presence of CMTM4. Binding of CXCL12 causes rapid internalization and lysosomal degradation of CXCR4 (Marchese, 2014). While the ~45 kDa species of the WT and the N180A mutant disappeared after CXCL12 exposure, the CXCR4 N15A and N15A/N180A mutants were resistant to CXCL12-mediated degradation, suggesting that complete CXCR4 glycosylation is essential for ligand binding (Figure 5D). However, the interaction with CMTM4 was not affected by removal of the main CXCR4 N15 glycosylation site (Figure 5E). Inhibition of lysosomal degradation by addition of chloroquine increased CXCR4 protein levels, indicating that CXCR4 is constantly degraded even in the absence of CXCL12. Chloroquine also interfered with the CMTM4-induced reduction of CXCR4 protein levels,

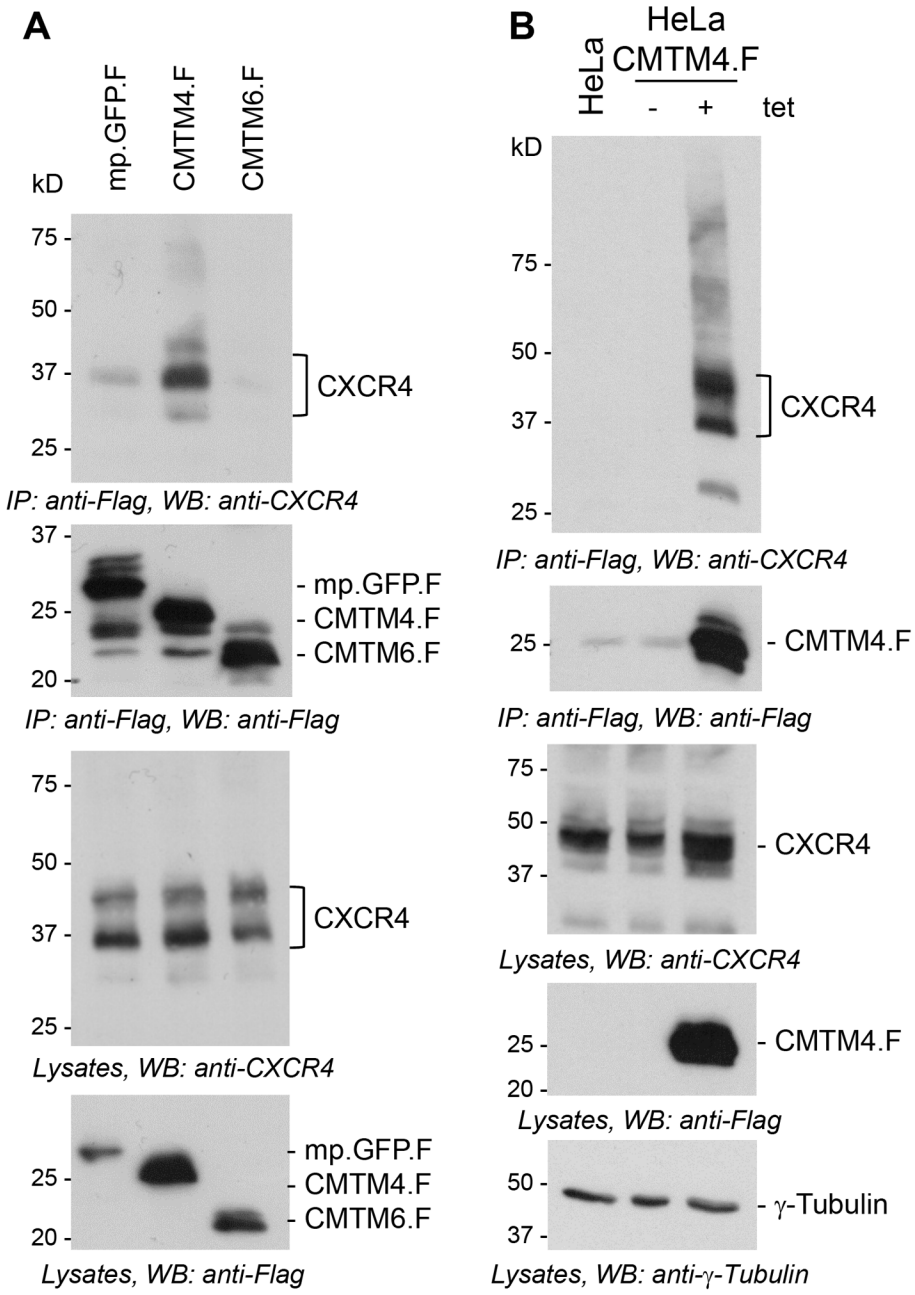

FIGURE 2: CMTM4 interacts with CXCR4. (A) CXCR4 coimmunoprecipitated with CMTM4.F, but not with CMTM6.F, in HEK 293T cells. M2 beads directed against Flag were used to precipitate CMTM proteins. Membrane-targeted myristoylated-palmitoylated GFP.F (mp.GFP.F) was used as negative control. (B) CMTM4.F interacted with endogenous CXCR4 in HeLa cells. A CMTM4.F-expressing HeLa cell line was used to determine the interaction of CMTM4 with endogenous CXCR4. CMTM4.F was affinity-purified using M2 beads. CXCR4 was detected in the eluate, using an anti-CXCR4 antibody. The antibody light chain with a molecular weight of 25 kDa was detected in the eluates. No CXCR4 was detected in the eluates of the negative controls.

suggesting that CMTM4 promotes lysosomal degradation of glycosylated CXCR4 (Supplemental Figure S4).

CMTM4 slows CXCR4 trafficking

Because members of the CMTM family were implicated in regulating cell surface expression of PD-L1 (Burr *et al.*, 2017; Mezzadra *et al.*, 2017), we determined the basal internalization rate of CXCR4 by measuring the residual cell surface CXCR4 using an anti-CXCR4 antibody in combination with a fluorescently labeled secondary antibody to detect cell surface CXCR4 in vivo. Expression of CMTM4 did not influence the basal internalization rate of CXCR4 in HeLa cells (Figure 6, A and B); CMTM4 also did not affect the decline of CXCR4 protein levels in the presence of cycloheximide (20 µg/ml for 16 h) (Figure 6C), suggesting that CMTM4 does not alter CXCR4 internalization and degradation in the absence of its ligand CXCL12. To determine whether CMTM4 affects CXCR4 before reaching the plasma membrane, we fused CXCR4-GFP, which has been shown to maintain its functional integrity (Tarasova *et al.*, 1998), to four conditional aggregation domains (CADs) (Thuenauer *et al.*, 2014). The CAD-CXCR4-GFP aggregate accumulates in the ER but is released upon addition of D/D-solubilizer, a membrane-permeable solubilizer. We then tracked CXCR4 in HEK 293T cells through the biosynthetic pathway until it appeared at the cell surface after the CADs were removed in the Golgi by furin-mediated cleavage. Comparison with mCherry revealed that CMTM4 significantly slowed the appearance of CXCR4-GFP at the cell surface (Figure 7, A–D). However, after 16 h the amount of surface CXCR4-GFP was no longer different from that of control cells (Supplemental Figure S5). Thus, CMTM4 overexpression slows CXCR4 trafficking from the ER to the plasma membrane but does not prevent CXCR4 from reaching the cell surface. CMTM4 and CXCR4 colocalized during their transport to the cell surface (Supplemental Figure S6). Costaining of CMTM4 with Golgin-97 revealed that CMTM4 accumulated in the Golgi of MCF7 cells (Supplemental Figure S7). To confirm these findings in vivo, we depleted *cmtm4* using MOs in the *cxcr4b:tFT* zebrafish line (Dona *et al.*, 2013). In this system, the newly synthesized proteins display mainly green fluorescence, whereas the proportion of red fluorescence increases with protein age (Dona *et al.*, 2013). While in the control group (*control MO*) the newly synthesized Cxcr4b was predominantly localized to the cell membranes of the pLLP with some of the aged, red fluorescent Cxcr4b found in intracellular vesicles, in the MO-depleted group (*cmtm4 MO*) both the newly synthesized and the aged Cxcr4b were found in intracellular vesicles (Figure 7E). Thus, Cmtm4 alters the subcellular localization of Cxcr4b in the zebrafish pLLP.

CMTM4 affects CXCL12-induced events

To determine whether CMTM4 affects the trafficking of CXCR4 in the presence of its ligand, we examined the CXCL12-induced

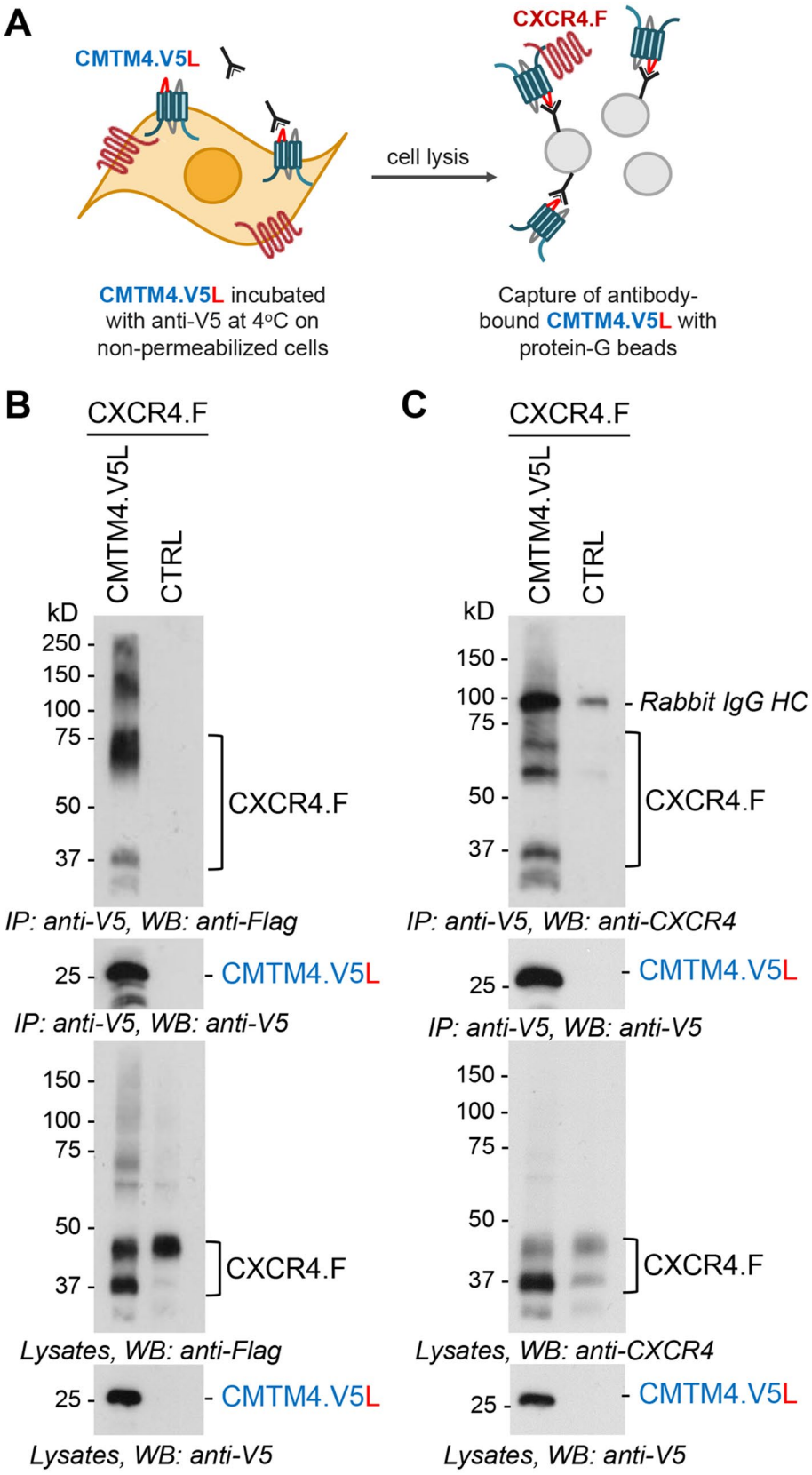

FIGURE 3: CXCR4 interacts with CMTM4 on the cell surface. (A) Diagram depicting the experimental approach. Nonpermeabilized cells, expressing CMTM4 with a V5-tag inserted into the first extracellular loop (CMTM4.V5L), were incubated with anti-V5 antibodies to precipitate CMTM4 from the cell surface. Interacting CXCR4 was subsequently analyzed by Western blot. (B) Cell surface CMTM4.V5L was precipitated with a rabbit anti-V5 antibody. HEK 293T cells, expressing only CXCR4.F and incubated with the same antibody, were used as negative control. After lysis, the antibody-bound proteins were purified using protein G Dynabeads. Lysates and eluates were analyzed by Western blot. CXCR4 was detected with a mouse anti-Flag antibody. (C) Restain with an anti-CXCR4 antibody confirmed that CMTM4.V5L interacted with higher-molecular-weight CXCR4 species as well as with ~37 kDa CXCR4.

internalization and degradation of CXCR4. CXCL12 triggered a rapid decrease of CXCR4 protein levels, which was partially attenuated in the presence of CMTM4 (Figure 8A). However, CMTM4 did not reduce fully glycosylated CXCR4 protein levels in HeLa cells as observed in HEK 293T cells. Tetracycline did not affect the CXCL12-mediated decrease of CXCR4 protein levels in HeLa WT cells, excluding potential unspecific tetracycline effects (Supplemental Figure S8A). Fluorescence-activated cell sorting (FACS) analysis of cell surface CXCR4 in the presence of its ligand confirmed that CMTM4 interferes with the CXCL12-induced internalization of CXCR4 (Figure 8B). To determine whether the reduced CXCR4 response to CXCL12 affects the activation of downstream signaling pathways, we analyzed typical CXCR4 targets in the presence of CMTM4. CMTM4 expression had no effect on activation of ERK1/2 (Supplemental Figure S8B), suggesting that CMTM4 does not prevent ligand binding. In contrast, the CXCL12-mediated AKT activation was significantly reduced in the presence of CMTM4 (Figure 8C).

CMTM4 is negatively correlated with CXCR4 in cancer

CXCL12/CXCR4 signaling has been linked to tumorigenesis, metastasis, and poor survival of patients with various cancers (Guo *et al.*, 2016; Shi *et al.*, 2020). CMTM family members have been portrayed as both oncogenes and tumor suppressors (Wu *et al.*, 2020). Analyzing 864 patients with various types of renal cancer of The Cancer Genome Atlas (TCGA) collection revealed that expression of CXCR4 is inversely correlated with survival ($p = 0.0012$), while high CMTM4 expression is associated with increased survival ($p < 0.0001$). While CXCR4 and CMTM4 were inversely correlated ($p < 0.0001$), CXCR4 and CXCR7/ACKR3 displayed positive correlation (Supplemental Figure S9A). In contrast, CMTM6 expression has no effect on survival rates in renal cancer ($p = 0.96$). To support the negative correlation between CXCR4 and CMTM4, we analyzed

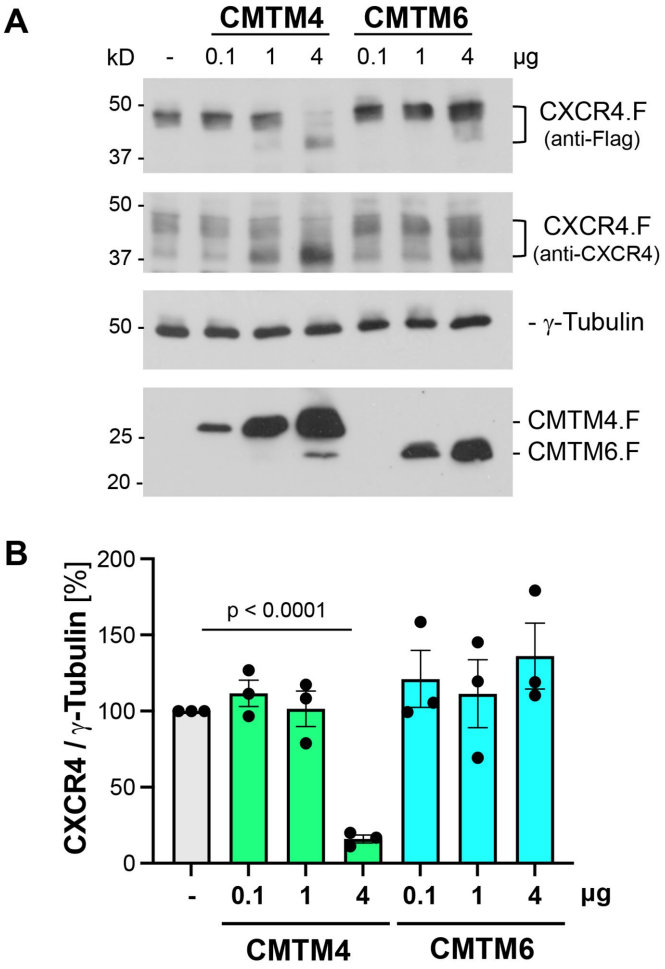

FIGURE 4: CMTM4 affects CXCR4 protein levels. (A) HEK 293T cells were cotransfected with 4 µg of Flag-tagged CXCR4 and increasing concentrations of Flag-tagged CMTM4 and CMTM6. Western blot analysis revealed a decrease in CXCR4 levels in the presence of 4 µg of CMTM4, while CXCR4 was not affected by CMTM6. (B) The high-molecular-weight band of CXCR4 from three independent experiments was quantified by densitometry using LabImage 1D. The protein levels of CXCR4.F detected by the anti-Flag antibody were normalized to γ-Tubulin. The quantification was performed in relation to the control sample with CXCR4 alone (*t* test; $p < 0.0001$).

tumor cell lines generated from transgenic *Vhl-/-/Trp53-/-/Rb1-/-* mice (Harlander *et al.*, 2017). While a negative correlation ($R = -0.89$, $p = 0.033$) was found between Cmtm4 and Cxcr4 in tumor cell lines, no correlation was found between Cmtm6 and Cxcr4 (Supplemental Figure S9B).

cmtm4 depletion disrupts Cxcr4b-dependent collective cell migration

To address the question of how CMTM4 deficiency might influence CXCR4-dependent cell migration programs, we depleted *cmtm4* in zebrafish embryos using MOs and monitored the lateral line formation by time-lapse video microscopy. The shape of the migrating pLLP in *cmtm4* MO (*cmtm4* MO)-treated embryos changed, the migration was retarded, and cells were leaving the pLLP cell cluster (Figure 9A; Supplemental Movies 1 and 2). To test whether *cxcr4* trafficking is responsible for these phenotypes, we exposed zebrafish embryos to Cxcl12a after depletion of *cmtm4* while monitoring migration of the pLLP. Ubiquitous Cxcl12a expression was induced in the *hsp70:cxcl12a; cldnb:lyn-GFP* zebrafish line by heat shock. Cxcl12 expression strongly enhanced the phenotype observed after *cmtm4* depletion. Cxcl12a altered the shape of the migrating pLLP in *cmtm4* MO-treated embryos and caused cells to separate from the cell cluster (Figure 9B; Supplemental Movies 3–5). Consistent with these findings, the pLLP of *cmtm4*$^{\Delta 60/\Delta 60}$ zebrafish embryos appeared to disintegrate, and no neuromast deposition was observed (Supplemental Figure S10). A similar phenotype was observed in embryos injected with higher concentration of *cmtm4* MO (Supplemental Figure S10). These observations suggest that altered trafficking of Cxcr4b disrupts the integrity of the pLLP in the absence of *cmtm4*, disrupting collective cell migration and allowing cells to respond individually to Cxcl12a.

DISCUSSION

CMTM4 and CMTM6 were originally identified as regulators of PD-L1 expression (Burr *et al.*, 2017; Mezzadra *et al.*, 2017). Our findings suggest that CMTM4, and likely also CMTM6, serve much broader functions in cargo trafficking and regulation of cell surface proteins. Prompted by the observation that mutation or depletion of *cmtm4* interferes with normal lateral line development in zebrafish embryos, we examined the interaction between CMTM4 and CXCR4 because the seven-membrane spanning receptor Cxcr4b plays an important role in coordinating the directed cell migration of the pLLP. Our findings suggested that Cmtm4 is involved in orchestrating the Cxcr4b gradient in the zebrafish pLLP. We therefore examined whether CXCR4 and CMTM4 can form a complex. Because the employed antibodies were not sensitive enough to detect CMTM4 in CXCR4-expressing cell lines, CXCR4-expressing HeLa cells were constructed to express CMTM4 in response to tetracycline. Endogenous CXCR4 coprecipitated with induced CMTM4, confirming the results obtained in HEK 293T cells (see Figure 2). CXCR4 accumulates in cholesterol-rich domains/lipid rafts at the cell surface (Wysoczynski *et al.*, 2005), which is likely also the case for MARVEL proteins such as CMTM4 (Cheong *et al.*, 1999). Immunoprecipitations of membrane-spanning, lipid-associated surface molecules are notoriously difficult; however, we included an ultracentrifugation step to remove incompletely solubilized membrane fragments to identify a direct interaction between CMTM4 and CXCR4. To determine whether CMTM4 is present at the cell surface, we inserted a V5 tag into the first extracellular loop and precipitated CMTM4 from nonsolubilized cells. This approach immobilized a higher-molecular-weight species of CXCR4, detected by anti-Flag as well as by anti-CXCR4 antibodies (see Figure 3, B and C). Higher-molecular-weight CXCR4 species have been reported in CXCR4-positive cell lines (Lapham *et al.*, 1999, 2002) but were not detected after precipitation of total CXCR4 from either HEK 293T or HeLa cells, suggesting that CMTM4 interacts with additional CXCR4 versions at the cell surface. Despite the similarity between CMTM4 and CMTM6, mainly CMTM4 and not CMTM6 was identified as an interactor of CXCR4, affecting its trafficking and stability. CMTM4 shifted the molecular weight of CXCR4 from ~45 kDa to ~37 kDa (see lane 4 in Figure 4A). Treatment of CXCR4 with PNGase F, removing N-linked glycosylation, indicated that CMTM4 promotes the accumulation of a partially glycosylated CXCR4, or alternatively targets CXCR4 for partial deglycosylation. Chloroquine, interfering with acidification of the lysosomal compartment, restored the ~45 kDa species but also increased the ~37 kDa species even in the absence of CMTM4 (see lane 3 in Supplemental Figure S4). Biosynthesis of N-glycans in the secretory pathway is initiated in the ER, followed by extensive modifications of the carbohydrate moieties in

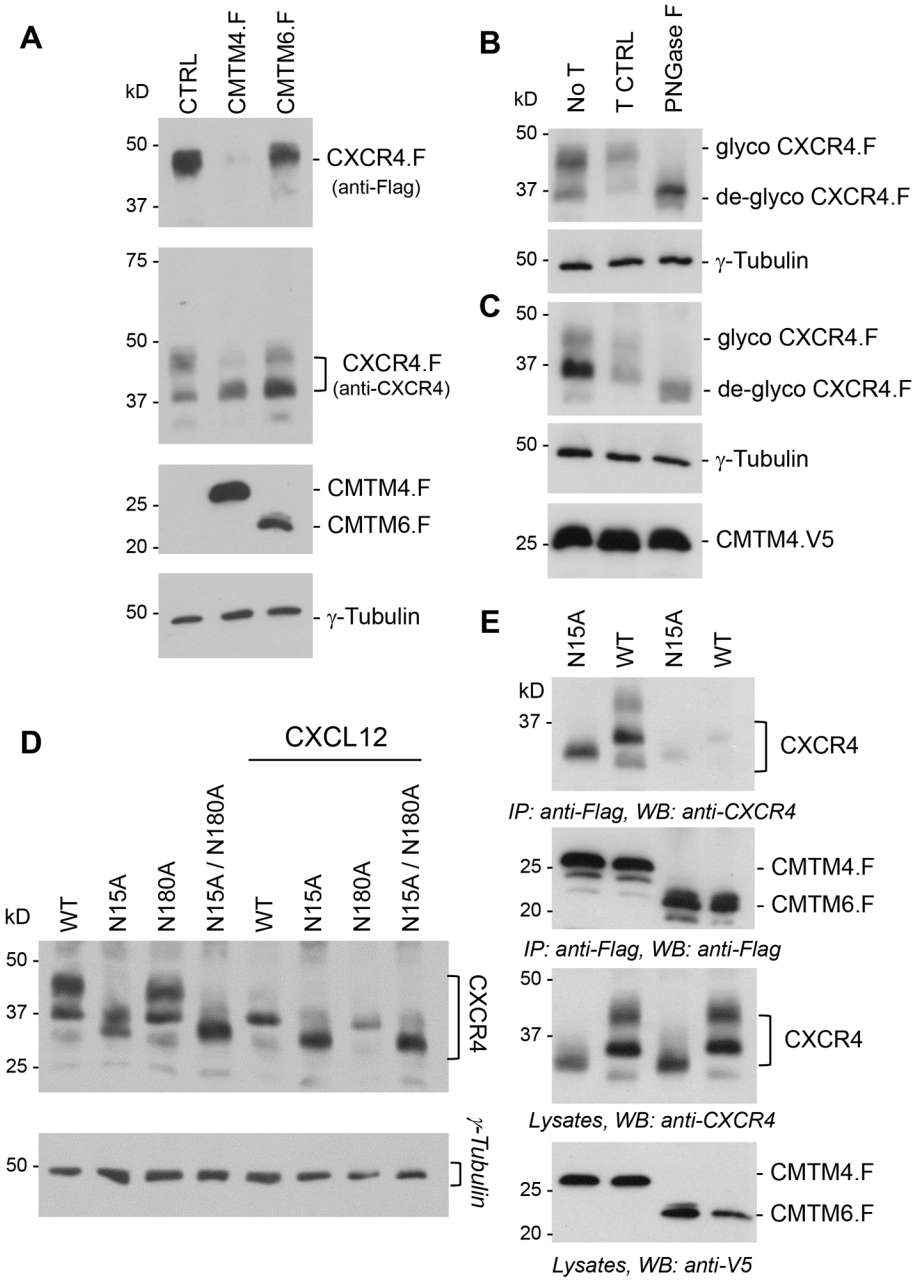

FIGURE 5: CXCR4 N-glycosylation is reduced in the presence of CMTM4. (A) CMTM4 almost completely abolished the ~45 kDa species of CXCR4, detected by anti-Flag, and increased the ~37 kDa species of CXCR4, detected by anti-CXCR4. The effect of CMTM6 on the shift from the ~45 to the ~37 kDa species was less pronounced. (B) CXCR4 is N-glycosylated in HEK 293T cells. CXCR4-expressing HEK 293T cell lysates were incubated with PNGase F, an enzyme that removes all N-linked glycosylation for 24 h at 37°C. Untreated (No T) lysates and lysates incubated under the same conditions without PNGase F (T CTRL) were used as controls. PNGase F reduced the molecular weight of CXCR4. (C) CXCR4 remains partially glycosylated in the presence of CMTM4. Cell lysates were treated as before. PNGase F lowered the molecular weight of CXCR4 slightly more than CMTM4. (D) Glycosylation of CXCR4 at the N-terminus is essential for CXCL12-mediated degradation. HEK 293T cells, expressing WT CXCR4 or the CXCR4 glycosylation mutants N15A, N180A, and N15A N180A, were exposed to 125 nM CXCL12 for 30 min. Only fully glycosylated WT and N180A CXCR4 responded to ligand-mediated degradation and a reduction of CXCR4 protein levels. (E) CMTM4 interacted with WT and N15A mutant CXCR4, indicating that N-glycosylation of CXCR4 is not required for CMTM4/CXCR4 interaction. HEK 293T cells were transfected as indicated. CMTM proteins were precipitated with anti-Flag; immobilized CXCR4 was detected by anti-CXCR4.

the *cis*- to *trans*-Golgi network (Reily *et al.*, 2019; Agliarulo and Parashuraman, 2022). Particularly, the *trans*-Golgi network and vesicles, arising from this compartment, are acidic (Anderson and Pathak, 1985). Thus, chloroquine could prevent maturation of the N-glycan attached to CXCR4 by preventing their exit from the Golgi. CMTM4, which is present in the Golgi (see Supplemental Figure S7), could act in a similar manner, retaining CXCR4 in the Golgi before complete maturation of its N-linked carbohydrate chains. Alternatively, CXCR4 could return from lysosomes to the Golgi apparatus and undergo partial deglycosylation to initiate another round of trafficking, which is prevented in the presence of chloroquine. CXCR4 is constantly internalized even in the absence of ligand (see Figure 6). Fully glycosylated CXCR4 expressed at the cell surface could escape ubiquitin-mediated lysosomal degradation in the presence of chloroquine, explaining the accumulation of the ~45 kDa CXCR4 species. It is less likely that CXCR4 is partially deglycosylated in lysosomes exposed to chloroquine because the breakdown of N-linked glycans in lysosomes requires extensive prior proteolysis, which is prevented by chloroquine (Winchester, 2005).

Using CADs to synchronize the release of CXCR4 from the ER (Thuenauer *et al.*, 2014), we observed that CMTM4 slowed the biosynthetic pathway to the cell surface (see Figure 7) without affecting overall surface expression of CXCR4 (see Supplemental Figure S5). Testing whether the altered trafficking of CXCR4 to the cell surface affects its function, we examined CXCR4-mediated signaling events in HeLa cells. While ERK1/2 phosphorylation after exposure to CXCL12 was not affected (see Supplemental Figure 8), AKT activation was dampened. AKT, but not ERK1/2, activation requires CXCR4 internalization (English *et al.*, 2018). Although CMTM4 did not affect the basal internalization or degradation of CXCR4, the CXCL12-induced endocytosis of CXCR4 was attenuated in CMTM4-expressing HeLa cells (see lane 4 in Figure 8A). The subcellular distribution of CMTM4, the changes in the CXCR4 glycosylation pattern, and the impact on CXCR4 signaling indicate that CMTM4 acts at multiple levels during the biosynthetic pathway of CXCR4.

CXCR4 and CMTM family members have been implicated in cancer. While CXCR4 has been linked to increased tumor invasion and metastasis, the role of

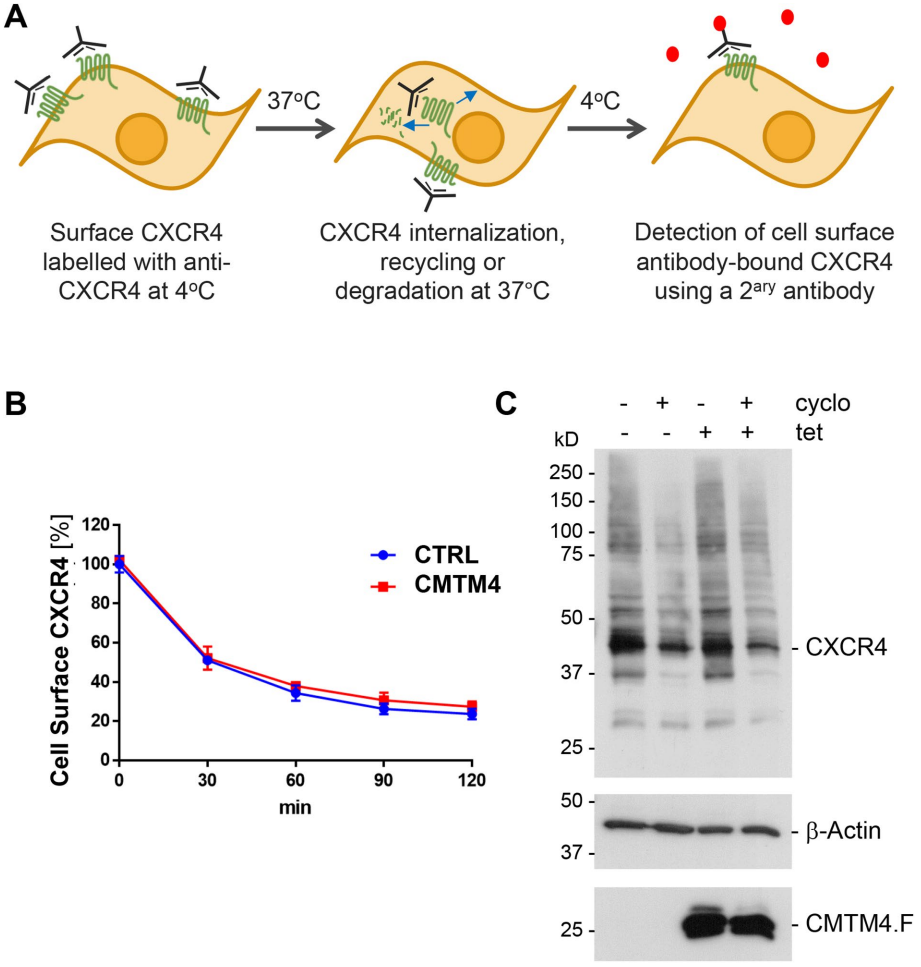

FIGURE 6: Basal internalization and degradation of CXCR4 is not affected by CMTM4. (A) Diagram of the CXCR4 internalization assay. (B) The time course of the basal internalization of CXCR4 in the absence of ligand did not reveal an effect of CMTM4 in HeLa cells. The percentage of CXCR4-positive cells remaining at the plasma membrane at the indicated time points was determined by FACS analysis. CMTM4.F expression was induced with 0.125 µg/ml tetracycline for 4 d. Error bars: mean ± SD. Each point represents three biological replicates. (C) Western blot analysis of the basal degradation of CXCR4 in the absence of ligand stimulation in non-induced or tetracycline-induced CMTM4.F-expressing HeLa cells, treated with cycloheximide (20 µg/ml) for 16 h. Depicted is one out of three experiments.

CMTM4 in cancer remains unclear. As a regulator of PD-L1 expression, decreased expression of CMTM4 appears to favor tumor-directed immune responses (Mezzadra *et al.*, 2017). Conversely, increased CMTM4 may inhibit CXCR4 expression and signaling and positively influence tumor-dependent survival. In renal cell cancers, high CXCR4 and low CMTM4 expression were associated with reduced survival (see Supplemental Figure S9). This inverse relationship supports the hypothesis that CXCR4 promotes renal cell cancer in the absence of CMTM4. In zebrafish embryos, depletion of *cmtm4* disrupted the integrity of the pLLP in response to Cxcl12a, allowing cells to separate from the cell cluster (see Figure 9) and thus resembling cell behavior observed during tumor metastasis.

Our findings indicate that CMTM4, and likely other CMTM family members, control trafficking not only of PD-L1, but also of other integral membrane proteins such as CXCR4 at multiple steps during the biosynthetic pathway, including their availability for ligand interactions at the cell surface and their responses to ligand stimulation.

MATERIALS AND METHODS

Request a protocol through *Bio-protocol*.

Cell culture

HEK 293T cells (American Type Culture Collection, Manassas, VA), HeLa cells (NIH AIDS Research and Reference Reagent Program operated by McKesson BioServices, Rockville, MD), and MCF-7 cells were routinely tested to exclude mycoplasma contamination. All cell lines were cultivated in DMEM supplied with 10% fetal bovine serum (FBS). For experiments in starvation conditions, the cells were cultivated in DMEM without FBS. HEK 293T cells were transiently transfected using the calcium phosphate method. Cell lysis was done 24 h later. To generate the tetracycline-inducible HeLa CMTM4.F overexpression cell line, CMTM4.F was cloned into the lentiviral vector pLVTH and cotransfected together with the plasmids encoding for viral packaging and envelope formation in HEK 293T cells. Virus, harvested 72 h after transfection, was added to HeLa cells, expressing the tTR-KRAB protein hybrid (Deuschle *et al.*, 1995). The process was repeated twice to increase the efficiency of the transduction. Tetracycline, added at a concentration of 0.125 µg/ml for 96 h to sequester tTR-KRAB and to allow tetO-dependent expression, resulted in optimal CMTM4.F levels. The MCF-7 eGFP.CMTM4 overexpression cell line was generated by two cycles of lentiviral transduction of MCF-7 wt cells as described above.

Plasmids

Human CXCR4 was obtained from the BIOSS Toolbox (https://www.bioss.uni-freiburg.de/de/toolbox/projects-services/cloning-service/) and cloned into a pcDNA6 vector with or without a C-terminal Flag tag for transient expression. The CXCR4 N15A, CXCR4 N180A, and CXCR4 N15A N180A glycosylation mutants were created by Quick Change Mutagenesis. Human CMTM4 was obtained from Source Bioscience (I.M.A.G.E. clone ID: 7939524) and cloned into a pcDNA6 vector with a C-terminal Flag tag or a C-terminal V5 tag. CMTM4.F was cloned into a pLVTH vector for lentivirus production. To generate an MCF-7 cell line constitutively expressing CMTM4 with an eGFP tag, the CMTM4 sequence was cloned into a pLVTH vector with N-terminal eGFP for lentivirus production. The CMTM4.V5L construct was synthesized by General Biosystems. The human CMTM6 sequence was obtained from Sino Biological (Eschborn, Germany; HG11340-M) and cloned into a pcDNA6 vector with a C-terminal Flag tag. The GFP construct with the myristoylated-palmitoylated sequence for plasma membrane targeting (mpGFP.F) was cloned into a pcDNA6 vector with a C-terminal Flag tag. The auxiliary plasmids for lentivirus production pCMV delta R. 8.91 and pMD-2-VSVg were gifts from Didier Trono (School of Life Sciences, Ecole Polytechnique Fédérale de Lausanne, Lausanne, Switzerland) (Wiznerowicz and Trono, 2003). All plasmids generated in this study were sequenced by Sanger sequencing, and the sequences are available upon request.

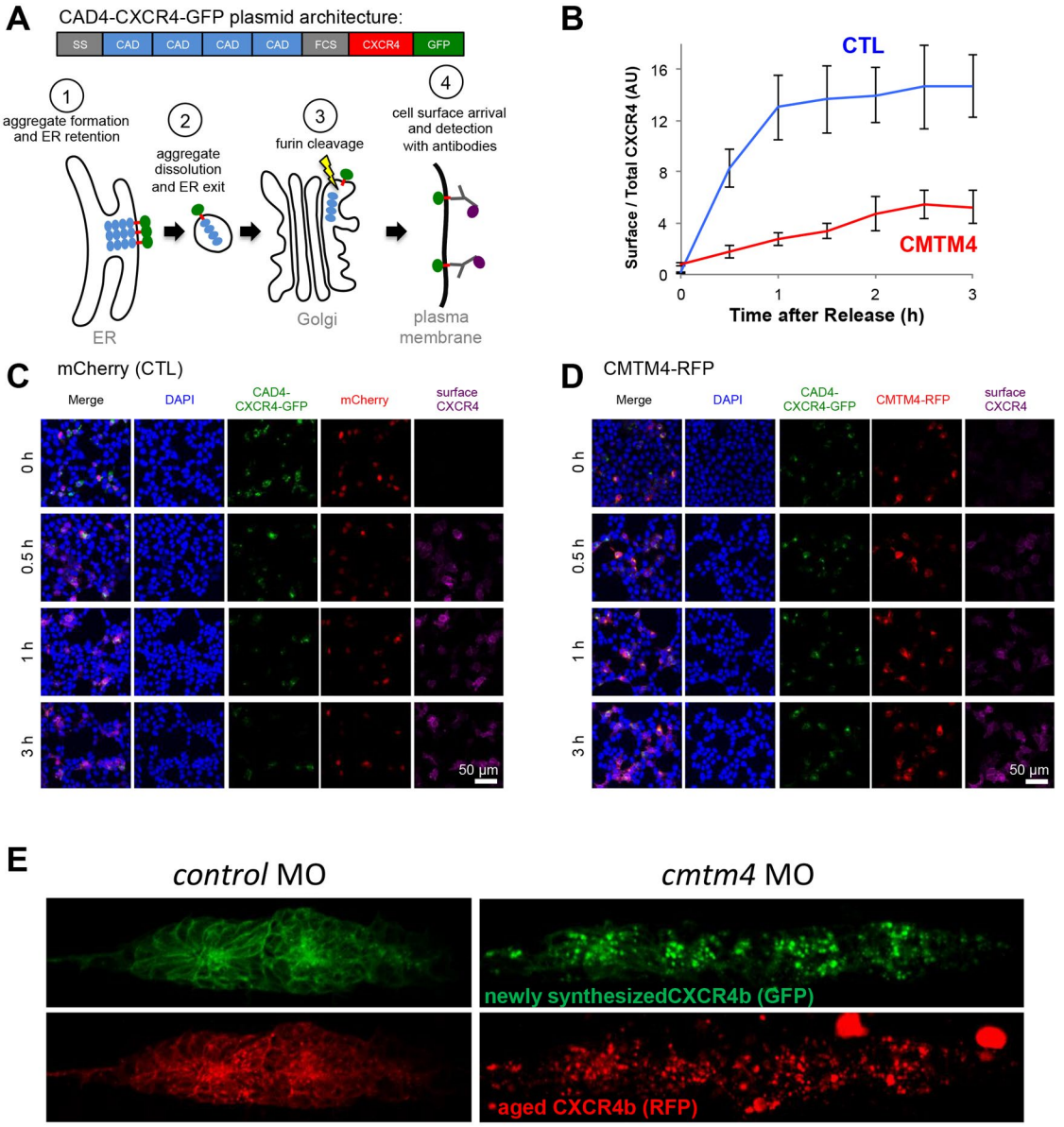

FIGURE 7: Coexpression of CMTM4 slows biosynthetic transport of CXCR4. (A) To study the biosynthetic route of CXCR4 in live cells, CXCR4 was fused to GFP to track cytoplasmic CXCR4 and to four CADs (Thuenauer *et al.*, 2014). The CAD4-CXCR4-GFP fusion protein encodes for a signal sequence (SS) that ensures insertion into the ER membrane. The CADs form aggregates that are retained in the ER after synthesis (step 1). The CAD4-CXCR4-GFP aggregates are dissolved by a membrane-permeable small molecule (D/D-solubilizer), which results in synchronous ER exit (step 2). The CADs are removed in the Golgi by furin via a furin cleavage site (FCS) (step 3). Antibodies are used to detect CXCR4 at the cell surface (step 4). To measure the kinetics of CXCR4 cell surface arrival, HEK 293 cells grown on fibronectin-coated glass slides were transfected with CAD4-CXCR4-GFP in combination with mCherry (CTL) or CMTM4-RFP. CAD4-CXCR4-GFP was released over the course of 3 h as indicated. To detect CXCR4-GFP at the cell surface, live cells were incubated with Alexa 647–conjugated anti-CXCR4 antibodies for 15 min. After fixation, cells were stained with 4′,6-diamidino-2-phenylindole (DAPI) to stain nuclei. (B) The graph shows the time course of CXCR4-GFP cell surface arrival in cells coexpressing mCherry (CTL) (blue line) and CMTM4-RFP (red line) calculated from the mean ratio of surface CXCR4 (determined from the anti-CXCR4 surface staining signal) and total CXCR4 (determined from the CXCR4-GFP signal) of >17 individual cells per time point and condition; error bar represents SEM. (C, D) Representative images from the cell surface arrival detection experiment. The images obtained by confocal microscopy show maximum intensity projections (MIP) of DAPI (blue), CAD4-CXCR4-GFP (green), mCherry or CMTM4-RFP (red), and the signal from cell surface CXCR4-GFP detected via antibodies (magenta). (E) Expression of Cxcr4b can be monitored over time in the *cxcr4b:tFT* zebrafish line (Dona *et al.*, 2013). In the control group (*control MO*) Cxcr4b is predominantly localized to the cell membranes of the pLLP. After MO depletion (*cmtm4 MO*), Cxcr4b was mislocalized to intracellular vesicles.

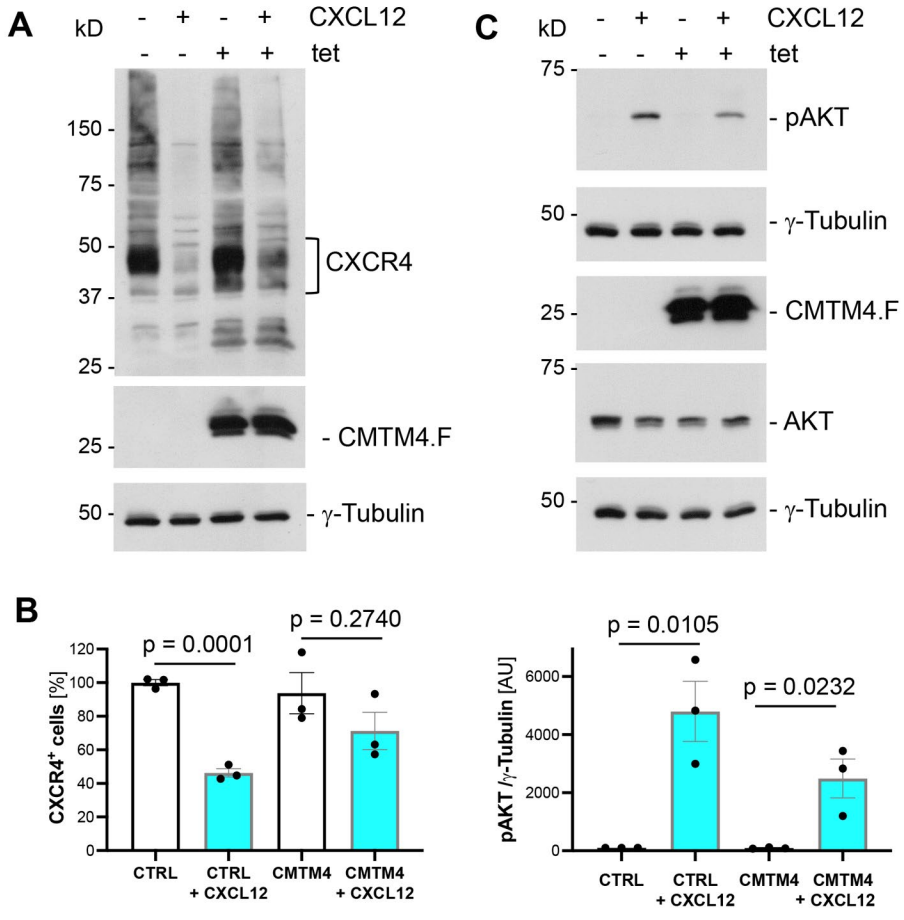

FIGURE 8: CMTM4 affects ligand-induced internalization and ligand-induced, CXCR4-mediated AKT activation. (A) CMTM4 expression, using the tetracycline-inducible HeLa cell line, attenuated the reduction of CXCR4 protein levels in response to CXCL12 (125 nM for 5 min). Depicted is one of three experiments. (B) FACS analysis of CXCR4 cell surface expression after CXCL12 stimulation (125 nM, 30 min). The ligand-induced internalization of CXCR4 is reduced in CMTM4.F-expressing HeLa cells (*t* test, mean ± SEM). (C) AKT activation is reduced after stimulation of tetracycline-inducible expression of CMTM4.F in HeLa cells treated with CXCL12 (125 nM for 5 min). Total and phosphorylated AKT protein levels were analyzed by Western blot in serum-free media. The band intensity of pAKT was measured by densitometry using LabImage 1D and normalized to γ-Tubulin (AU, artificial unit; *t* test, mean ± SEM).

PNGase F deglycosylation assay

The deglycosylation assay was performed according to the manufacturer's instructions for nondenaturing conditions. Briefly, lysates were mixed with 2 ml of glycobuffer2 and 2 µl of 10% NP-40 (New England Biolabs, Ipswich, MA; P0704S) in a final volume of 20 µl. PNGase F (2 µl) was added for 24 h at 37°C. Control samples were treated as described above without the addition of PNGase F (T control). Untreated samples (No T) were used as a second control.

Protein extraction and Western blot

Cell lysis and protein extraction were done using RIPA buffer (13.7 mM Na_2HPO_4, 6.3 mM NaH_2PO_4, 1% Triton X-100, 0.1% SDS, 150 mM NaCl, 50 mM NaF, 2 mM EDTA, 0.5% sodium deoxycholate) supplied with fresh protease inhibitors (Complete protease inhibitor cocktail tablets from Roche, Mannheim, Germany; 11697498001; Na_3VO_4 from Sigma-Aldrich, St. Louis, MO; S6508). For the detection of phosphorylated proteins, phosphatase inhibitors (PhosSTOP from Roche; 04906837001, β-glycerophosphate from Sigma-Aldrich, St. Louis, MO; G9422) were additionally supplied. Cell debris was removed by centrifugation at 18,000 × *g* for 30 min at 4°C. The protein concentration was determined using the DC-protein Micro-Assay kit (Biorad, Hercules, CA; 500-0112). Total lysates supplied with dithiothreitol (DTT)-containing Laemmli buffer (6× solution: 375 mM Tris, pH 6.8, 10% SDS, 36% glycerol, 10–20 mg of bromophenol blue, 0.6 M DTT) were loaded on 8–12% polyacrylamide gels and separated by SDS–PAGE followed by semidry transfer on polyvinylidene fluoride (PVDF) membranes. Milk (5%) or bovine serum albumin (BSA) (5%) was used for blocking, followed by incubation with primary antibodies overnight at 4°C or for 1 h at room temperature (RT). Proteins were detected by chemiluminescence using horseradish peroxidase–conjugated secondary antibodies. Quantification was done by densitometry using the software LabImage 1D (Intas Science Imaging, Goettingen, Germany). The density measurement of all proteins of interest was normalized to γ-Tubulin levels to account for differences in sample loading. Primary antibodies used for Western blot were as follows: rabbit anti-AKT (Cell Signaling Technology, Danvers, MAA; #9272), rabbit anti-pAKT (Cell Signaling Technology, Danvers, MA; #4060), rabbit anti-ERK1/2 (Cell Signaling Technology, Danvers, MA; #4695), rabbit anti-pERK1/2 (Cell Signaling Technology, Danvers, MA; #4370), rabbit anti-CXCR4 (Abcam, Cambridge, UK; ab124824), mouse anti-Flag (Sigma-Aldrich, St. Louis, MO; F3165), rabbit anti-V5 (Chemicon, Limburg an der Lahn, Germany; AB3792), mouse anti-V5 (Bio-Rad Serotec, Oxford, UK; MCA1360), mouse anti–γ-tubulin (Sigma-Aldrich, St. Louis, MO; T6557), and mouse anti–β-actin (Sigma-Aldrich, St. Louis, MO; A1978).

Cell surface arrival assay

The assay was performed as previously described (Thuenauer *et al.*, 2014; Stroukov *et al.*, 2019). Briefly, cells were transfected for 6 h and then treated with 100 µg/ml cycloheximide for 1 h. D/D-solubilizer was applied for 3 h.

Coimmunoprecipitation

HEK 293T, HeLa wt, or HeLa CMTM4.F cells treated with or without 0.125 µg/ ml tetracycline for 4 d were lysed in immunoprecipitation (IP) buffer (20 mM Tris, pH 7.5, 50 mM NaCl, 50 mM NaF, 0.1 mM EDTA, pH 8.0, 15 mM $Na_4P_2O_7$, 1% Triton X-100) supplied with fresh protease inhibitors as mentioned above. The lysates were incubated on ice for 45 min. After centrifugation at 18,000 × *g* for 15 min at 4°C, the supernatant was collected, and a second centrifugation was performed at 100,000 × *g* for 30 min at 4°C to separate the solubilized proteins (supernatant) from the insoluble membrane fraction. The protein concentration was measured as mentioned above. Part of the lysates was stored in DTT-containing Laemmli buffer for Western blot analysis. For immunoprecipitation of Flag-tagged proteins,

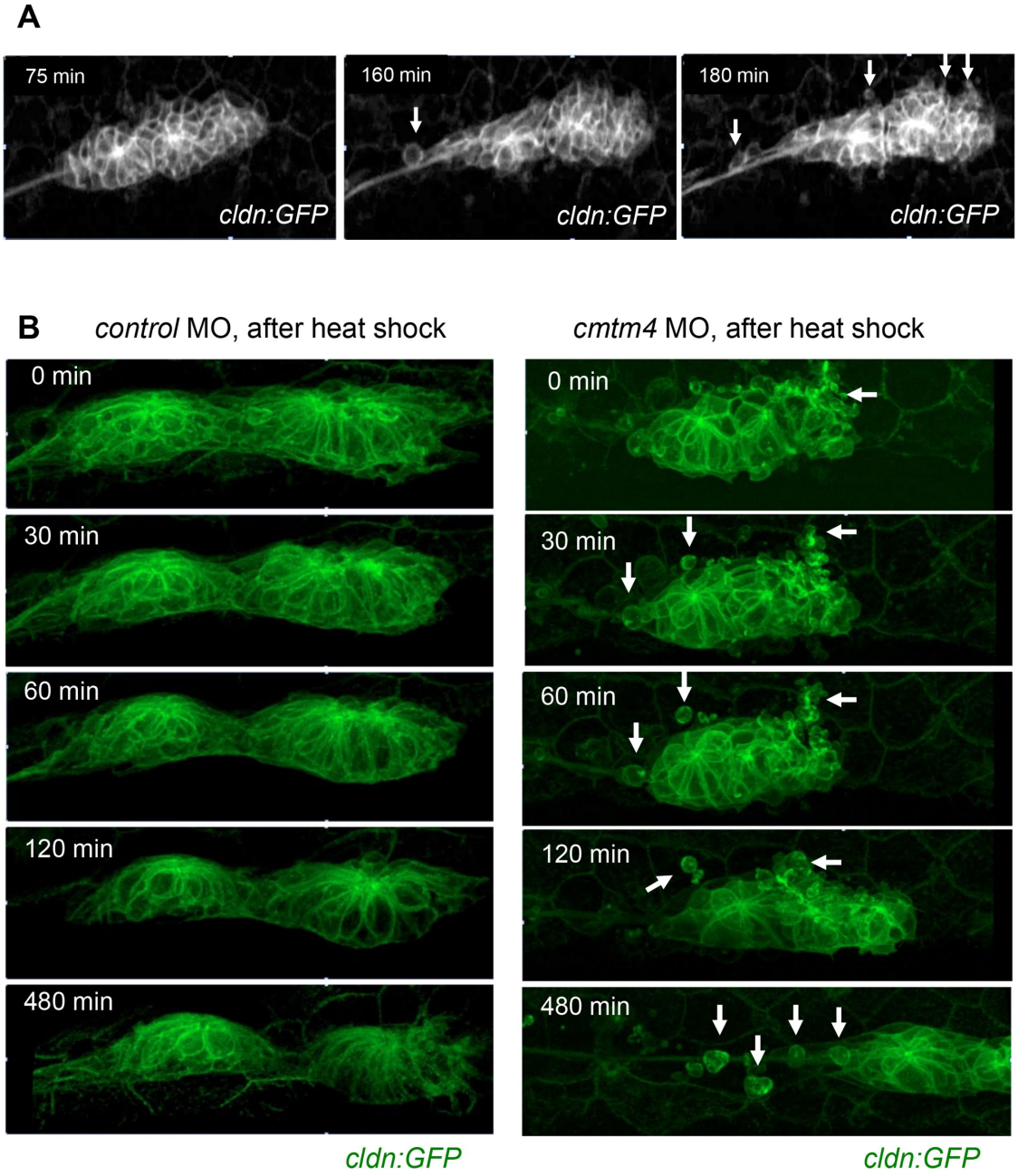

FIGURE 9: Depletion of *cmtm4* alters the integrity of the migrating pLLP cell cluster. (A) Cells separating from the pLLP cell cluster were observed after *cmtm4* depletion (2 ng). Frames were taken from a time-lapse movie at the times indicated (see Supplemental Movies 1 and 2). (B) The decreased cohesiveness of the pLLP cell cluster was aggravated after heat shock–mediated Cxcl12a generation. Ubiquitous expression of Cxcl12a was triggered using the *hsp70:cxcl12a* in combination with a heat shock (38°C for 45 min). While the effect in zebrafish embryos treated with control MO (*ctrl* MO, 2 ng) was transient, ubiquitous Cxcl12a production altered the shape of the migrating pLLP in *cmtm4* MO–treated embryos and caused cells to separate from the migrating cell cluster (arrows). The depicted frames were taken from a time-lapse movie (see Supplemental Movies 3–5).

the rest of the lysates was incubated with anti-Flag M2 agarose beads (Sigma-Aldrich, St. Louis, MO; A2220) for 1.5 or 16 h at 4°C on rotation. For immunoprecipitation of CXCR4, the lysates were incubated with protein G Sepharose beads (VWR, Radnor, PA; 17-0618-01) preconjugated to an anti-CXCR4 antibody (BD Pharmingen, San Diego, CA; 551852) for 2 h at 4°C on rotation. Subsequently, the beads were washed three to five times with IP buffer. Elution was done with 70 µl of 1.5× Laemmli buffer with DTT. The eluates were heated at 42°C for 30 min and stored at –20°C for subsequent analysis by Western blot.

Cell surface coimmunoprecipitation

The protocol for cell surface coimmunoprecipitation was adjusted from Burr *et al.* (2017). Briefly, HEK 293T cells transiently expressing CXCR4.F and CMTM4.V5L were washed once with ice-cold phosphate-buffered saline (PBS) and collected using a detachment solution containing 10 mM EDTA in PBS. The cells were pelleted at 300 × *g*, 5 min, 4°C, resuspended in PBS supplied with 2% BSA, and incubated on ice for 1 h with a rabbit anti-V5 antibody (Chemicon Millipore, Limburg an der Lahn, Germany; AB3792) or a rat anti-CXCR4 antibody (BD Pharmingen, San Diego, CA; 551852). After

two washing steps with PBS containing 2% BSA to remove unbound antibody, the cells were lysed in IP buffer supplied with fresh protease inhibitors as described above. The lysates were incubated on ice for 45 min followed by a centrifugation step at 18,000 × *g*, 15 min, 4°C. The protein concentration of the postnuclear supernatant was determined as mentioned above, and 50 µl of the lysates was stored in Laemmli buffer with DTT. The lysates were incubated with protein G Dynabeads (Invitrogen, Waltham, MA; 10003D) for 2 h at 4°C, rotating to capture antibody-bound CMTM4.V5L or CXCR4.F. Subsequently, the beads were washed four times on rotation at 4°C with IP buffer to remove unbound proteins. Elution was done as described above.

CXCR4 cell surface expression after ligand stimulation

HeLa CMTM4.F cells treated with or without 0.125 µg/ml tetracycline for 4 d were incubated with or without 125 nM CXCL12 (Biomol, Hamburg, Germany; 94842) for 30 min at 37°C to trigger ligand-induced internalization of CXCR4. The cells were placed on ice, washed once with ice-cold PBS, and scraped from the plates with 1 ml of PBS containing 10 mM EDTA and 1% sodium azide. The cells were pelleted by centrifugation at 300 × *g*, 5 min, 4°C, resuspended in PBS supplied with 2% BSA, and incubated with a mouse phycoerythrin (PE)-conjugated anti-CXCR4 antibody (R&D Systems, Minneapolis, MN; FAB170P-100) on ice for 30 min. The cells were washed with PBS containing 2% BSA to remove unbound antibody and resuspended in 1 ml of the same solution, and the cell surface expression of CXCR4 in each sample was analyzed by flow cytometry.

Internalization assay

The CXCR4 internalization assay was performed as described in Burr *et al*. (2017). Briefly, HeLa CMTM4.F cells treated with or without 0.125 µg/ml tetracycline for 4 d were washed once with ice-cold PBS and scraped from the plates with a PBS solution containing 10 mM EDTA. A sample of noninduced cells was collected separately to be used as negative control for nonspecific binding of the secondary antibody. The cells were pelleted by centrifugation at 300 × *g*, 5 min, 4°C, and resuspended in a solution containing 2% BSA in PBS. The samples were incubated on ice with a rat monoclonal anti-CXCR4 antibody (BD Pharmingen, San Diego, CA; 551852) for 45 min and then washed twice with the same buffer to remove unbound antibody. The tetracycline-induced and noninduced cells were resuspended in DMEM + 10% FBS and incubated in a water bath for 30, 60, 90, or 120 min to allow internalization of antibody-bound CXCR4. One tetracycline-induced and one noninduced sample were kept on ice to measure the CXCR4 cell surface expression at $t = 0$. At the indicated time points, the cells were placed on ice and cold PBS was added to prevent further endocytosis of the receptor. The samples were washed once more with PBS supplied with 2% BSA, resuspended in the same buffer, and incubated on ice with a mouse anti-rat IgG2b FITC-conjugated secondary antibody (BD Pharmingen, San Diego, CA; 553884) for 30 min. The cells were washed once more to remove unbound secondary antibody and finally resuspended in 1 ml of PBS supplied with 2% BSA. The CXCR4 cell surface expression in each sample was measured by flow cytometry.

Degradation assay

HeLa CMTM4.F cells treated with or without 0.125 µg/ml tetracycline for 4 d were treated with or without 20 µg/ml cycloheximide (Sigma-Aldrich, St. Louis, MO; D7698) for 16 h. The cells were washed once with ice-cold PBS, scraped from the plates using PBS supplied with 10 mM EDTA, and counted using an automated cell counter. Living cells (2.5×10^6) from each condition were lysed in RIPA buffer supplied with fresh protease inhibitors as described above. No protein measurement was done because the protein concentration of the cycloheximide-treated samples is much lower than that in the untreated samples due to protein degradation. For Western blot analysis of CXCR4 protein levels, the same volume of lysates in Laemmli buffer was loaded on the gel. β-Actin was used as a loading control as it has a longer half-life than γ-Tubulin.

Immunofluorescence staining

MCF-7 eGFP.CMTM4 cells were fixed and permeabilized with ice-cold MeOH for 5 min. The cells were blocked with 5% donkey serum for 1 h at RT and subsequently incubated with a mouse anti–Golgin-97 antibody (Invitrogen, Waltham, MA; A21270) for 1 h at RT. A donkey anti-mouse Cy3-conjugated secondary antibody (Jackson Immuno Research; 715-165-150) was used to detect the protein by immunofluorescence. The nuclei were stained with Hoechst 33342 dye (Molecular Probes; H-1399). Z stack images were obtained with an LSM 880 confocal microscope from ZEISS using a 63× oil objective. The immunofluorescence for Cxcr7 in zebrafish embryos was done as previously described (Dona *et al*., 2013).

Zebrafish lines and maintenance

Zebrafish lines were maintained and raised as previously described (Westerfield, 1995). All zebrafish (*Danio rerio*) husbandry was performed under standard conditions in accordance with national ethical and animal welfare guidelines approved by the ethics committee for animal experiments at the Regierungspräsidium Freiburg, Germany (permit number G-16/89). We used the following transgenic lines: *cldnb:lyn-GFP* (Haas and Gilmour, 2006), *cxcr4b:tFT* (Dona *et al*., 2013), *hsp70:cxcl12a* (Knaut *et al*., 2005), and $cmtm4^{\Delta 60/\Delta 60}$. $cmtm4^{\Delta 60/\Delta 60}$ was generated in this study using CRISPR/Cas9 gene editing. A guide RNA (gRNA) targeting the first exon of *cmtm4* (5′-TCTGGAGAGCACGGGCTCGG TGG-3′) was selected with the help of the online tool CHOPCHOP (http://chopchop.cbu.uib.no/) (Labun *et al*., 2016). gRNAs were synthesized using the MEGAshortscript T7 Transcription Kit (Thermo Fisher Scientific, Waltham, MA). Cas9 protein and the gRNAs were injected in zebrafish oocytes at the one-cell stage. F0 founders (zebrafish mosaic for the mutation in the germline) were identified using the following primers: forward 5′-GGCCACTCTTGTTTCTTGGG-3′; reverse 5′-GCAAAGCAGGCTCATAAGTTT-3′.

Morpholino oligonucleotides

cmtm4 splice blocking MO, *cmtm4-SBM* (5′-CCAAGACTACTTCAACTTTACCACTT-3′) targeting the first exon–intron junction of *cmtm4*, *cmtm4* translation blocking morpholino, *cmtm4-TBM* (5′-TCAGTCTCCTCGTTATTCCTCATGC-3′, a standard control MO (5′-CCTCTTACCTCAGTTACAATTTATA-3′), and a p53-targeting MO (5′-GCGCCATTGCTTTGCAAGAATTG-3′) were ordered at Gene Tools, Philomath, USA). Injection solution (4 nl) consisting of MOs diluted in 100 mM KCl, 10 mM HEPES (4-(2-hydroxyethyl)-1-piperazineethanesulfonic acid), and 0.1% phenol red (Sigma-Aldrich) were microinjected into fertilized oocytes at the one-cell stage. To reduce side effects, all MOs were coinjected with a p53-MO (Robu *et al*., 2007).

Whole mount in situ hybridization

Whole mount in situ hybridization (WISH) was performed as previously described (Thisse and Thisse, 2008). To prepare a *cmtm4* WISH probe, a PCR fragment was cloned in a TOPO vector (Invitrogen). The PCR was performed using a cDNA library from 1–2-d-old

embryos and the following set of primers: forward 5′-GTGGTTTTG-GCAGCTCTCAA-3′; reverse 5′-gactctcagcttcctccgtt-3′.

Heat shock–triggered Cxcl12a overexpression

Zebrafish embryos carrying the *hsp70:cxcl12a* transgene were heat-shocked for 45 min in a 38°C water bath. The heat-shocked embryos were embedded in 1% low-melting agarose for imaging. Time-lapse imaging was carried out on a ZEISS LSM 510 DUO with a 63×/1.2NA objectives. The embryos injected with the *cmtm4* and control MOs were simultaneously heat-shocked and imaged using multiwell dishes.

Time-lapse confocal imaging

Zebrafish embryos were anesthetized with a 0.01% tricaine solution and embedded in 1% low-melting agarose in four-well glass bottom dishes. Time-lapse imaging was carried out on a ZEISS LSM 510 DUO and Zeiss LSM 510 META with 40×/1.1NA and 63×/1.2NA objectives and 488, 543, and 561 nm laser lines.

Image analysis of *cxcr4b:tFT* lifetime ratios

Lifetime analysis was carried out as previously described (Dona *et al.*, 2013). Z stacks for *cxcr4b:tFT* imaging were obtained with a ZEISS LSM 510 DUO using a 63×/1.3NA objective and 488 and 561 nm laser lines.

Statistical analysis

Microsoft Excel and GraphPad Prism were used for statistical tests and graphs, depicting mean ± SEM unless otherwise indicated. Significance was determined using the unpaired, two-sided *t* test. The graphs in Figure 1C were generated using R (https://www.r-project.org/) as previously described (Dona *et al.*, 2013).

ACKNOWLEDGMENTS

We thank Darren Gilmour for providing the *cxcr4b:tFT* transgenic line and the Cxcr7 antibody. Special thanks go to Roland Nitschke and the staff of the Life Imaging Center (LIC) and Marie Follo and Dieter Herchenbach (Lighthouse Core Facility) for assistance and advice on image acquisition and FACS analysis. Many thanks to Didier Trono for the kind gift of the pCMV delta R. 8.91 and pMD-2-VSVg plasmids. We are grateful to Barbara Müller, Christina Engel, Annette Schmitt, and Carina Kramer for their excellent technical support. We thank the staff of the aquatic core facility (AquaCore, RI_00544) at the University Freiburg Medical Center–IMITATE, Germany, for excellent support with zebrafish maintenance and experimentation. This work was supported by the German Research Foundation (DFG) (WA 597/23-1 to G. W.), by the DFG under Germany's Excellence Strategy (CIBSS-EXC-2189-Project ID 390939984 to G. W.), by the Excellence Initiative of the German Research Foundation (EXC 294 and EXC 2189), a German Research Foundation grant (RO 4341/2-1) to W. R. and R. T., a grant from the Ministry of Science, Research and the Arts of Baden-Württemberg (Az: 33-7532.20) to W. R., and the Freiburg Institute for Advanced Studies (FRIAS) by a senior research fellowship to W. R.

REFERENCES

Agliarulo I, Parashuraman S (2022). Golgi apparatus regulates plasma membrane composition and function. Cells 11, 368.

Anderson RG, Pathak RK (1985). Vesicles and cisternae in the trans Golgi apparatus of human fibroblasts are acidic compartments. Cell 40, 635–643.

Burr ML, Sparbier CE, Chan YC, Williamson JC, Woods K, Beavis PA, Lam EYN, Henderson MA, Bell CC, Stolzenburg S, *et al.* (2017). CMTM6 maintains the expression of PD-L1 and regulates anti-tumour immunity. Nature 549, 101–105.

Busillo JM, Benovic JL (2007). Regulation of CXCR4 signaling. Biochim Biophys Acta 1768, 952–963.

Caballero A, Mahn SA, Ali MS, Rogers MR, Marchese A (2019). Heterologous regulation of CXCR4 lysosomal trafficking. J Biol Chem 294, 8023–8036.

Chabot DJ, Chen H, Dimitrov DS, Broder CC (2000). N-linked glycosylation of CXCR4 masks coreceptor function for CCR5-dependent human immunodeficiency virus type 1 isolates. J Virol 74, 4404–4413.

Cheong KH, Zacchetti D, Schneeberger EE, Simons K (1999). VIP17/MAL, a lipid raft-associated protein, is involved in apical transport in MDCK cells. Proc Natl Acad Sci USA 96, 6241–6248.

Dalle Nogare D, Chitnis AB (2017). A framework for understanding morphogenesis and migration of the zebrafish posterior Lateral Line primordium. Mech Dev 148, 69–78.

Deuschle U, Meyer WK, Thiesen HJ (1995). Tetracycline-reversible silencing of eukaryotic promoters. Mol Cell Biol 15, 1907–1914.

Donà E, Barry JD, Valentin G, Quirin C, Khmelinskii A, Kunze A, Durdu S, Newton LR, Fernandez-Minan A, Huber W, *et al.* (2013). Directional tissue migration through a self-generated chemokine gradient. Nature 503, 285–289.

English EJ, Mahn SA, Marchese A (2018). Endocytosis is required for CXC chemokine receptor type 4 (CXCR4)-mediated Akt activation and anti-apoptotic signaling. J Biol Chem 293, 11470–11480.

Guo F, Wang Y, Liu J, Mok SC, Xue F, Zhang W (2016). CXCL12/CXCR4: a symbiotic bridge linking cancer cells and their stromal neighbors in oncogenic communication networks. Oncogene 35, 816–826.

Haas P, Gilmour D (2006). Chemokine signaling mediates self-organizing tissue migration in the zebrafish lateral line. Dev Cell 10, 673–680.

Harlander S, Schönenberger D, Toussaint NC, Prummer M, Catalano A, Brandt L, Moch H, Wild PJ, Frew IJ (2017). Combined mutation in Vhl, Trp53 and Rb1 causes clear cell renal cell carcinoma in mice. Nat Med 23, 869–877.

Huskens D, Princen K, Schreiber M, Schols D (2007). The role of N-glycosylation sites on the CXCR4 receptor for CXCL-12 binding and signaling and X4 HIV-1 viral infectivity. Virology 363, 280–287.

Knaut H, Blader P, Strähle U, Schier AF (2005). Assembly of trigeminal sensory ganglia by chemokine signaling. Neuron 47, 653–666.

Labun K, Montague TG, Gagnon JA, Thyme SB, Valen E (2016). CHOPCHOP v2: a web tool for the next generation of CRISPR genome engineering. Nucleic Acids Res 44, W272–W276.

Lapham CK, Romantseva T, Petricoin E, King LR, Manischewitz J, Zaitseva MB, Golding H (2002). CXCR4 heterogeneity in primary cells: possible role of ubiquitination. J Leukoc Biol 72, 1206–1214.

Lapham CK, Zaitseva MB, Lee S, Romanstseva T, Golding H (1999). Fusion of monocytes and macrophages with HIV-1 correlates with biochemical properties of CXCR4 and CCR5. Nat Med 5, 303–308.

Marchese A (2014). Endocytic trafficking of chemokine receptors. Curr Opin Cell Biol 27, 72–77.

Mezzadra R, Sun C, Jae LT, Gomez-Eerland R, de Vries E, Wu W, Logtenberg MEW, Slagter M, Rozeman EA, Hofland I, *et al.* (2017). Identification of CMTM6 and CMTM4 as PD-L1 protein regulators. Nature 549, 106–110.

Nagasawa T, Hirota S, Tachibana K, Takakura N, Nishikawa S, Kitamura Y, Yoshida N, Kikutani H, Kishimoto T (1996). Defects of B-cell lymphopoiesis and bone-marrow myelopoiesis in mice lacking the CXC chemokine PBSF/SDF-1. Nature 382, 635–638.

Picard L, Wilkinson DA, McKnight A, Gray PW, Hoxie JA, Clapham PR, Weiss RA (1997). Role of the amino-terminal extracellular domain of CXCR-4 in human immunodeficiency virus type 1 entry. Virology 231, 105–111.

Reily C, Stewart TJ, Renfrow MB, Novak J (2019). Glycosylation in health and disease. Nat Rev Nephrol 15, 346–366.

Robu ME, Larson JD, Nasevicius A, Beiraghi S, Brenner C, Farber SA, Ekker SC (2007). p53 activation by knockdown technologies. PLoS Genet 3, e78.

Sadri F, Rezaei Z, Fereidouni M (2022). The significance of the SDF-1/CXCR4 signaling pathway in the normal development. Mol Biol Rep 49, 3307–3320.

Sánchez-Pulido L, Martín-Belmonte F, Valencia A, Alonso MA (2002). MARVEL: a conserved domain involved in membrane apposition events. Trends Biochem Sci 27, 599–601.

Shi Y, Riese DJ 2nd, Shen J (2020). The role of the CXCL12/CXCR4/CXCR7 chemokine axis in cancer. Front Pharmacol 11, 574667.

Staller P, Sulitkova J, Lisztwan J, Moch H, Oakeley EJ, Krek W (2003). Chemokine receptor CXCR4 downregulated by von Hippel-Lindau tumour suppressor pVHL. Nature 425, 307–311.

Stroukov W, Rösch A, Schwan C, Jeney A, Römer W, Thuenauer R (2019). Synchronizing protein traffic to the primary cilium. Front Genet 10, 163.
Tarasova NI, Stauber RH, Michejda CJ (1998). Spontaneous and ligand-induced trafficking of CXC-chemokine receptor 4. J Biol Chem 273, 15883–15886.
Thisse C, Thisse B (2008). High-resolution in situ hybridization to whole-mount zebrafish embryos. Nat Protoc 3, 59–69.
Thuenauer R, Hsu YC, Carvajal-Gonzalez JM, Deborde S, Chuang JZ, Romer W, Sonnleitner A, Rodriguez-Boulan E, Sung CH (2014). Four-dimensional live imaging of apical biosynthetic trafficking reveals a post-Golgi sorting role of apical endosomal intermediates. Proc Natl Acad Sci USA 111, 4127–4132.
Valentin G, Haas P, Gilmour D (2007). The chemokine SDF1a coordinates tissue migration through the spatially restricted activation of Cxcr7 and Cxcr4b. Curr Biol 17, 1026–1031.
Westerfield M (1995). The Zebrafish Book: A Guide for the Laboratory Use of Zebrafish, University of Oregon Press.
Winchester B (2005). Lysosomal metabolism of glycoproteins. Glycobiology 15, 1r–15r.
Wiznerowicz M, Trono D (2003). Conditional suppression of cellular genes: lentivirus vector-mediated drug-inducible RNA interference. J Virol 77, 8957–8961.
Wu J, Li L, Wu S, Xu B (2020). CMTM family proteins 1-8: roles in cancer biological processes and potential clinical value. Cancer Biol Med 17, 528–542.
Wysoczynski M, Reca R, Ratajczak J, Kucia M, Shirvaikar N, Honczarenko M, Mills M, Wanzeck J, Janowska-Wieczorek A, Ratajczak MZ (2005). Incorporation of CXCR4 into membrane lipid rafts primes homing-related responses of hematopoietic stem/progenitor cells to an SDF-1 gradient. Blood 105, 40–48.
Zhou H, Tai HH (1999). Characterization of recombinant human CXCR4 in insect cells: role of extracellular domains and N-glycosylation in ligand binding. Arch Biochem Biophys 369, 267–276.
Zou YR, Kottmann AH, Kuroda M, Taniuchi I, Littman DR (1998). Function of the chemokine receptor CXCR4 in haematopoiesis and in cerebellar development. Nature 393, 595–599.